

Seismic stability analysis of tunnel face in purely cohesive soil by a pseudo-dynamic approach

Qi Huang^a, Jin-feng Zou^{*} and Ze-hang Qian^b

School of Civil Engineering, Central South University,
No.22, Shaoshan South Road, Changsha, Hunan Province, People's Republic of China

(Received February 10, 2020, Revised July 27, 2020, Accepted August 22, 2020)

Abstract. To give a solution for seismic stability of tunnel faces subjected to earthquake ground shakings, the pseudo-dynamic approach is originally introduced to analyze tunnel face stability in this study. In the light of the upper-bound theorem of limit analysis, an advanced three-dimensional mechanism combined with pseudo-dynamic approach is proposed. Based on this mechanism, the required support pressure on tunnel face can be obtained by equaling external work rates to the internal energy dissipation and implementing an optimization searching procedure related to time. Both time and space feature of seismic waves are properly accounted for in the proposed mechanism. For this reason, the proposed mechanism can better represent the actual influence of seismic motion and has a remarkable advantage in evaluating the effects of vertical seismic acceleration, soil amplification factor, seismic wave period and initial phase difference on tunnel face stability. Furthermore, the pseudo-dynamic approach is compared with the pseudo-static approach. The difference between them is illustrated from a new but understandable perspective. The comparison demonstrates that the pseudo-static approach is a conservative method but still could provide precise enough results as the pseudo-dynamic approach if the value of seismic wavelengths is large or the height of soil structures is small.

Keywords: limit analysis; tunnel face; seismic; pseudo-dynamic; cohesive soils

1. Introduction

During the process of tunnel excavation, stability analysis of surrounding rocks (Wang *et al.* 2019, Li and Zou 2020, Aksoy *et al.* 2020) and tunnel faces (Zou and Zuo 2017, Li and Yang 2019, Qian *et al.* 2019, Xue *et al.* 2019) are two most critical issues, about which many contributions have been done. The present work only focuses on the latter issue. Among plenty of influencing factors to the tunnel face stability, the spatial variation of soil property, the pore water pressure and the seismic effects of an earthquake are the most important ones for their significant influence. The effects of two former factors have been investigated by many researchers and a lot of sensible results were achieved (Pan and Dias 2015, Zou and Qian 2018). On the contrary, the effects of earthquake motions on tunnel face stability are seldom studied. In fact, the occurrence of an earthquake could cause the tunnel face collapse, leading to heavy casualties and property losses. Especially in earthquake-prone areas, when the tunnel has a long construction period, the seismic effects deserve careful consideration in the preliminary design phase.

Saada *et al.* (2013) investigated the seismic destabilizing effects on a tunnel face by combining the classical Conical translational failure mechanism and Horn failure mechanism with the pseudo-static approach, respectively. Pan and Dias (2018) studied the seismic stability of a tunnel face driven in weak rock masses based on an advanced three-dimensional rotational failure mechanism and the pseudo-static method. However, there is still a lack of relevant research on the seismic tunnel face stability in purely cohesive soils. Strictly speaking, purely cohesive soils do not really exist in nature. When a tunnel is excavated in low-permeability soils, the soils ahead of the tunnel face tend to exhibit purely cohesive shear resistance ($\varphi=0$). Under such certain circumstance, the soils can be approximately regarded as the purely cohesive soils (Perazzelli and Anagnostou 2017). Therefore, the study of cohesive soils has practical significance.

With respect to the tunnel face collapse mechanism in purely cohesive soils, Mollon *et al.* (2013) proposed an ingenious three-dimensional continuous velocity field in the framework of kinematic approach. The concept of continuous velocity field was originally put forward by Osman *et al.* (2006) and Klar *et al.* (2007). Because the phenomenon observed in the centrifuge testing conducted by Schofield (1980) showed that undrained clay masses move towards tunnel face like a “flow” instead of a rigid movement, Mollon *et al.* (2013) applied the concept of continuous velocity field in the purely cohesive soils. Compared with existing mechanisms based on the upper-bound theorem, the mechanism on the basis of the three-dimensional continuous velocity field proposed by Mollon

*Corresponding author, Professor
E-mail: zoujinfeng_csu@163.com

^aPh.D. Student

E-mail: huangqi_csu@163.com

^bPh.D. Student

E-mail: 15200806569@163.com

et al. (2013) could provide the best upper-bound results. For this reason, it has inspired plenty of research works based on this mechanism to investigate the stability of tunnel face in purely cohesive soils and been validated to work well (Klar and Klein 2014, Zhang *et al.* 2017). In the present work, this mechanism would be extended to analyze the seismic influence.

About the consideration of seismic effects, the pseudo-static method is always popular both in research and practice (Liu *et al.* 2015, Zhang *et al.* 2017, Shukla and Jakka 2018, Sun and Dias 2019, Chen *et al.* 2020) for its easy-to-understand concept and easy-to-use feature. However, the pseudo-static method also has an obvious shortcoming that it couldn't properly reflect the time and spatial effect of the dynamic loading induced by an earthquake. The pseudo-static method treats the dynamic loading as time and spatial independent by defining the seismic acceleration as a constant which is uniform throughout the whole soil layer. To address this shortcoming, the pseudo-dynamic approach was proposed and is becoming widely accepted among investigators recently. Numerous contributions combined with the pseudo-dynamic approach have been done in analyzing the seismic stability of geotechnical engineering, including slopes (Qin and Chian 2017), retaining walls (Giri 2011), bridge abutments (Basha and Babu 2009), strip anchors (Ganesh *et al.* 2018) and so on. Hence, the introduction of a pseudo-dynamic approach into the seismic tunnel face stability analysis is absolutely necessary.

In the present study, based on the upper-bound theorem, the seismic tunnel face stability in purely cohesive soil is investigated by means of combining an advanced three-dimensional failure mechanism proposed by Mollon *et al.* (2013) with the pseudo-dynamic approach, which could represent the input earthquake in terms of horizontal and vertical accelerations varying with time and space. Numerical simulations are conducted to validate the mechanism. For the sake of comparison, the pseudo-static approach is also studied. The influence of earthquake on tunnel face stability and the differences between the pseudo-static approach and pseudo-dynamic approach are discussed detailedly. It should be emphasized that the main purpose of the present study is not to provide charts that could be directly used in practical engineering, but to give some preliminary insights into the impact of earthquakes on the tunnel face stability and all the numerical results obtained should thus be considered as such.

2. Advanced 3D failure mechanism

This section aims to introduce the advanced three-dimensional collapse failure mechanism based on the upper-bound theorem of limit analysis, which is widely used in analyzing geotechnical engineering (Zou *et al.* 2019, Chen *et al.* 2019, Qian *et al.* 2020) for its simple expression and rigorous theory. In the implementation of the upper-bound theorem, the most important part is the construction of a kinematically admissible velocity field. The closer the velocity field is to the actual situation, the better the solution would be. Then, on basis of the

developed velocity field, by equaling the total rate of external work to the rate of internal energy dissipation, a rigorous upper bound of the critical load of this failure system is obtained (Chen 1975). For purely cohesive soils, the Tresca yield criterion is satisfied, so the classic work equation can be expressed as follows:

$$\int_S T_i v_i dS + \int_V f_i v_i dV = \int_V 2c_u |\dot{\varepsilon}|_{max} dV + \int_{S_D} c_u |\Delta v_i| dS \quad (1)$$

where T_i is the surface force applied on the boundary S ; f_i is the body force applied on volume V ; v is the kinematically admissible velocity of the field; $|\dot{\varepsilon}|_{max}$ is the principal component of the plastic strain rate; c_u is the soil undrained cohesion; and Δv_i is the velocity jump across any discontinuity S_D . Note that T_i, f_i and v_i are vectors and others are scalars.

Next, the advanced three-dimensional failure mechanism proposed by Mollon *et al.* (2013) would be briefly described. Note that this mechanism is suitable for the condition of shield tunneling under compressed air and the support pressure applied on the tunnel face is regarded as uniformly distributed.

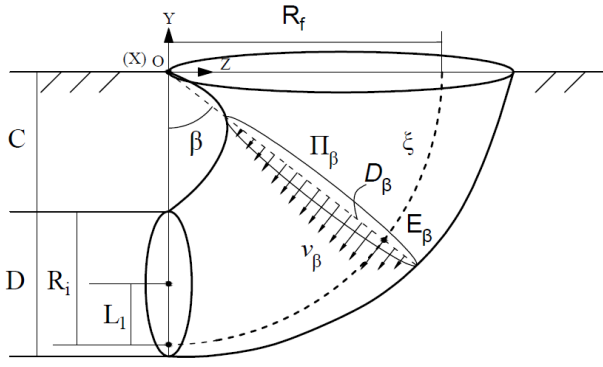
2.1 Three-dimensional continuous velocity field

Inspired by the concept of continuous velocity field and based on the centrifuge testing conducted by Schofield (1980), Mollon *et al.* (2013) proposed this three-dimensional continuous velocity field for tunnel face collapse in purely cohesive soils as shown in Fig. 1.

From Fig. 1, there is a tunnel with a diameter D and covered by upper soils in a depth C . The envelope of the whole tunnel face failure zone is a torus composed of circles with various diameters from the tunnel face to the ground surface. The three-dimensional continuous velocity field can be generated or described by the following steps:

(1) *Geometry.* Based on the observation in numerical simulations conducted by Mollon *et al.* (2013), the maximal velocity on the tunnel face is located at the bottom position. Hence, in Fig. 1(a), the maximal velocity point in this velocity field is assumed downwards at a distance L_1 ($=0.4D$) below the center of tunnel face. Then the arc ζ whose radius is $C+0.9D$ around the center O is regarded as the maximal velocity line. Furthermore, at any plane Π_β decided by angle β (angle between the vertical direction and the plane Π_β), the location of maximal velocity point is assumed similar as the tunnel face, namely that the maximal velocity point is located at a distance $0.4D_\beta$ away from the center of a circle Π_β . Therefore, when the value of β is 0, the R_i of plane Π_β which is the tunnel face is $0.9D$; when the value of β is $\pi/2$, the R_f of plane Π_β which is the ground surface is $C+0.9D$; when the value of β ranges from 0 to $\pi/2$, the R_β of plane Π_β changes linearly from R_i to R_f along with the arc ζ . In this way, the geometry of this failure zone is determined.

(2) *Coordinate system.* To better describe this velocity field, a special curvilinear coordinate system including three



(a) Three-dimensional continuous velocity field

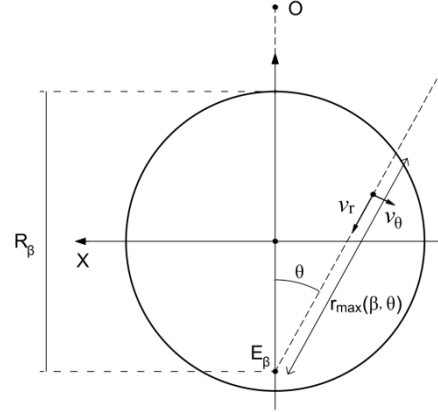
(b) Components of the velocity field in Plane Π_β

Fig. 1 Layout of the velocity field for purely cohesive soils

dimensions β , θ and r is established. In Fig. 1(a), the β can determine a plane Π_β . At the plane Π_β , taking the maximal velocity point E_β as an origin of a common polar coordinate system, any point at this plane can be easily described by angle θ and distance r as shown in Fig. 1(b).

(3) *Velocities*. Based on the curvilinear coordinate system, the vector of velocity also has three components v_β , v_θ and v_r . The direction of v_β is perpendicular to plane Π_β while v_θ and v_r at the plane Π_β are orthoradial and radial components respectively. Moreover, because the velocity field is continuous, there should be no velocity discontinuity among these three components. As shown in Fig. 1(a), the v_β is assumed to have a maximal value at point E_β and decrease to zero at the edge of failure body in a parabolic way. Meanwhile, the velocity flux across any plane Π_β is assumed as constant. In plane Π_β , the v_θ is regarded as negligible and assumed to be zero at any point. Then, on account of normality condition that no volume change occurs in soil plastic deformation ($\text{div}(\varepsilon) = 0$), the v_r is determined finally. By this means, all vectors of velocity in this mechanism can be calculated.

Due to the complicated calculation process of v_β and v_r , a discretization program is conducted in Matlab environment to do this work. Fig. 2(a) shows a three-dimensional view of this mechanism and Fig. 2(b) is the mesh used in this discretization analysis. From Fig. 2(b), it can be seen that the envelope of the meshed area is a quarter of a torus with a constant radius R_f . The failure body is entirely incorporated in this mesh area. Three dimensions β , θ and r are divided into N_β , N_θ and N_r blocks respectively. For clearer illumination, the mesh of schematic diagram in Fig. 2 is very coarse and discretization parameters are $N_\beta = 6$, $N_\theta = 12$ and $N_r = 5$ respectively. The actual mesh used in computation program is much finer and the chosen values of N_β , N_θ and N_r are 90, 90 and 200 respectively, which can well balance the accuracy of calculation and the computational time. Moreover, to avoid large gradient, the mesh is refined so that the mesh in the area of large velocity

is relatively dense and the mesh in the area of small velocity is relatively sparse. Through this way, any element bounded by six curved facets $S_1, S_2, S_3, S'_1, S'_2$ and S'_3 like Fig. 2(b) can be described by coordinate $P(\beta, \theta, r)$ and velocity vector $v(v_\beta, v_\theta, v_r)$. All the work equations in the following parts are based on this discretization technique.

2.2 Work equation

According to the three-dimensional continuous velocity field, the work equation can be established, i.e., the Eq. (1). Each term of Eq. (1) should be fully analyzed. The external surface forces include the support pressure applied on the tunnel face (σ_t) and the possible surcharge loading applied on the ground surface (σ_s). The external body forces consist of the soil gravity and the seismic forces in both horizontal and vertical directions. The internal energy dissipation only involves the deformation of the soil mass because there is no velocity discontinuity in this continuous velocity field. Hence, Eq. (1) can be rewritten as

$$\dot{W}_{\sigma_t} + \dot{W}_{\sigma_s} + \dot{W}_\gamma + \dot{W}_{k_h} + \dot{W}_{k_v} = \dot{D} \quad (2)$$

where \dot{W}_{σ_t} is the work rate of the tunnel face pressure σ_t ; \dot{W}_{σ_s} is the work rate of the ground surface surcharge σ_s ; \dot{W}_γ is the work rate of the soil weight γ ; \dot{W}_{k_h} and \dot{W}_{k_v} are the work rates of the horizontal and vertical seismic forces, respectively; and \dot{D} is the internal energy dissipation rate.

The work rate generated by seismic forces would be specifically investigated in **Section 3**. Except that, the other terms in Eq. (2) can be calculated as follows: The work rate of the support pressure on tunnel face is formulated by

$$\dot{W}_{\sigma_t} = -\sigma_t \cdot \sum_{N_r, N_\theta, \beta=0} (v_\beta \cdot S_3) \quad (3)$$

The work rate of the surcharge loading on ground surface is formulated by

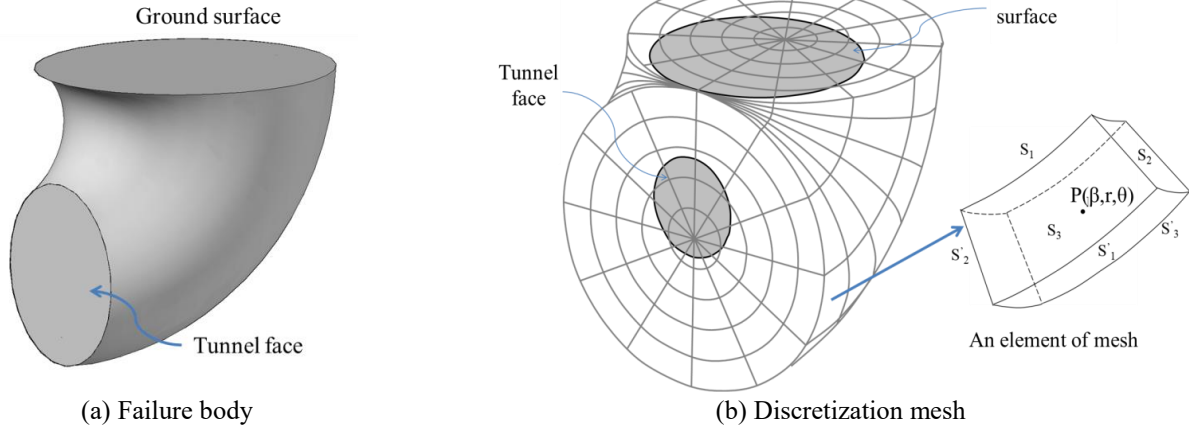


Fig. 2 Discretization of the mechanism

$$\dot{W}_{\sigma_s} = \sigma_s \cdot \sum_{N_r, N_\theta, \beta=\pi/2} (v_\beta \cdot S'_3) \quad (4)$$

The work rate of the soil gravity is expressed by

$$\dot{W}_\gamma = \gamma \cdot \sum_{N_\beta, N_r, N_\theta} (v_\gamma \cdot \delta V) \quad (5)$$

The internal energy dissipation produced by the soil deformation can be presented as

$$\dot{D} = c_u \cdot \sum_{N_\beta, N_r, N_\theta} (2 \cdot \max(|\dot{\varepsilon}_i|) \cdot \delta V) \quad (6)$$

where v_γ is the vertical component of velocity under Cartesian coordinate system; δV is the volume of a meshed element; c_u is the soil undrained cohesion; S_3 and S'_3 are the areas of the curved facets of a discretized element; and $\max|\dot{\varepsilon}_i|$ is the maximum of the principal strain rate component.

The detailed derivations of Eqs. (3)-(6) can be seen in Mollon *et al.* (2013) if the readers are interested. Then, to finish Eq. (2), the work rate of seismic forces in this advanced three-dimensional failure mechanism should be calculated in a proper approach and this is what the following section involves.

3. Kinematic analysis with a pseudo-dynamic approach

This section aims to incorporate the seismic effect into the tunnel face stability analysis in the framework of kinematic approach. In most geotechnical engineering stability analyses, the conventional pseudo-static approach is classically adopted to complete the evaluation. Assuming that the seismic effect is time-independent, the pseudo-static approach simply regards the dynamic loading induced by an earthquake as a constant value, i.e., the pseudo-static inertia force. Also, this pseudo-static inertia force is uniformly distributed throughout the whole geotechnical engineering. Obviously, these assumptions of pseudo-static approach are

far from the actual situation. As is well known, the seismic effect on geotechnical engineering comes from the seismic waves, including the primary wave and the shear wave. The primary wave and the shear wave are time-dependent and the inertia forces induced by these waves alternate in direction and magnitude. Hence, the pseudo-dynamic approach which describes the seismic motion with a sinusoidal function can better represent the influence of earthquakes.

Next, the pseudo-dynamic approach would be investigated and be incorporated into the kinematic analysis in **Section 2** to analyze the tunnel face stability in purely cohesive soils. For the sake of comparison, the pseudo-static approach would also be investigated.

3.1 Pseudo-dynamic stability analysis

The pseudo-dynamic approach considers both the primary wave and the shear wave generated by earthquakes. When the primary wave is propagating through the geotechnical engineering, the displacement of soil particles occurs in the same direction of propagation of the wave. However, when the shear wave is propagating through the geotechnical engineering, the displacement of soil particles occurs in an orthogonal direction of propagation of the wave. If an earthquake happens, both the primary wave and the shear wave would propagate from the bottom of the engineering to the top. Therefore, the passage of the primary and shear waves would cause the horizontal and vertical displacements of soil mass, respectively. The propagating velocity of primary wave V_p in soils can be calculated by

$$V_p = \sqrt{\frac{2G(1-\nu)}{\rho(1-2\nu)}} \quad (7)$$

where G is the shear modulus of soils, ρ is the soil density and ν is the soil Poisson's ratio. The propagating velocity of shear wave in soils V_s can be calculated by

$$V_s = \sqrt{\frac{G}{\rho}} \quad (8)$$

In the present work, the property of soils is regarded as

homogeneous, i.e., the variations of G , ρ and ν are considered as negligible. According to Das (1993), for most geological materials, the ratio of V_p to V_s can be taken as 1.87. Besides, it is assumed that the primary wave and the shear wave share the same seismic period T . Actually, for most of the geotechnical structures, the seismic period T is taken as 0.3s (Prakash 1981).

In addition, Steedman and Zeng (1990) conducted dynamic centrifuge tests and found that the seismic acceleration is amplified as the waves propagate from the bottom of the soil layers to the top. Consequently, the amplification phenomenon should be taken into account in the investigation. The influence factors of this amplification involve the primary and shear wave velocities, the primary and shear wave periods and the properties of soil materials such as damping, elastic modulus and shear modulus. This amplification is difficult to be described in a precise way, but for simplicity, an amplification factor f is defined to account for it.

Based on the analysis above, using a sinusoidal function correlated with time, the seismic accelerations induced by the primary wave and the shear wave can be expressed as

$$\begin{cases} a_h(h_i, t) = \left[1 + \frac{h_i}{H}(f-1) \right] k_h g \sin 2\pi \left(\frac{t}{T} - \frac{h_i}{TV_s} \right) \\ a_v(h_i, t) = \left[1 + \frac{h_i}{H}(f-1) \right] k_v g \sin 2\pi \left(\frac{t}{T} - \frac{h_i}{TV_p} + \frac{t_0}{T} \right) \end{cases} \quad (9)$$

where $a_h(h_i, t)$ and $a_v(h_i, t)$ are the horizontal and vertical seismic accelerations at any height h_i and time t , respectively; k_h and k_v are the horizontal and vertical seismic acceleration coefficients, respectively; H is the height from the bottom of whole geotechnical engineering to the top; h_i is the height above the bottom of the engineering for any considered i th element; f is the amplification factor; g is the acceleration due to gravity; and t_0 is the initial time phase difference between the horizontal and vertical accelerations at the bottom of the engineering and its value ranges from $-T$ to T . Note that the TV_s and TV_p are exactly the wavelengths of the shear wave and primary wave and can be denoted as λ_s and λ_p , respectively.

Combined with the discretization technique and Cartesian coordinate system, the horizontal and vertical seismic accelerations of any described element in the continuous velocity field can be obtained by Eq. (9). In Eq. (9), the H and h_i are calculated by

$$H = C + D \quad (10)$$

$$h_i = C + D + y_i \quad (11)$$

Then, the work rates generated by seismic forces on a discretized element can be expressed as

$$\begin{cases} \delta \dot{W}_{kh} = m_i \cdot a_h(i) \cdot v_h(i) \\ \delta \dot{W}_{kv} = m_i \cdot a_v(i) \cdot v_v(i) \end{cases} \quad (12)$$

where $\delta \dot{W}_{kh}$ and $\delta \dot{W}_{kv}$ are the work rates of horizontal and vertical seismic forces on a discretized element,

respectively; m_i is the mass of the i th element; and $v_h(i)$ and $v_v(i)$ are the horizontal and vertical components of the i th element velocity vector, respectively.

Substituting Eqs. (9)-(11) into Eq. (12), Eq. (12) can be rewritten as

$$\begin{cases} \delta \dot{W}_{kh} = \gamma_i \cdot \delta V \cdot \left[1 + \frac{C+D+y_i}{C+D} \cdot (f-1) \right] \cdot k_h \cdot \sin 2\pi \left(\frac{t}{T} - \frac{C+D+y_i}{TV_s} \right) \cdot v_z \\ \delta \dot{W}_{kv} = \gamma_i \cdot \delta V \cdot \left[1 + \frac{C+D+y_i}{C+D} \cdot (f-1) \right] \cdot k_v \cdot \sin 2\pi \left(\frac{t}{T} - \frac{C+D+y_i}{TV_p} + \frac{t_0}{T} \right) \cdot v_y \end{cases} \quad (13)$$

Summing the work rates of every element, the total work rates of seismic accelerations are given by

$$\begin{cases} \dot{W}_{kh} = \sum_{N_\beta, N_\gamma, N_\theta} (\delta \dot{W}_{kh}) \\ \dot{W}_{kv} = \sum_{N_\beta, N_\gamma, N_\theta} (\delta \dot{W}_{kv}) \end{cases} \quad (14)$$

Substituting Eqs. (3)-(6) and Eq. (14) into Eq. (2) and after some simplifications, the critical collapse support pressure σ_t can be obtained by

$$\sigma_t = \sigma_s \cdot N_s + \gamma \cdot D \cdot N_\gamma - c_u \cdot N_c + k_h \cdot \gamma \cdot D \cdot N_{kh} + k_v \cdot \gamma \cdot D \cdot N_{kv} \quad (15)$$

where N_s , N_γ , N_c , N_{kh} and N_{kv} are the coefficients corresponding to surcharge loading, soil weight, cohesion, horizontal seismic acceleration and vertical seismic acceleration, respectively. These coefficients are dimensionless parameters and can be expressed as

$$N_s = \frac{\sum_{N_\beta, N_\theta, \beta=0} (v_\beta \cdot S'_3)}{\sum_{N_\beta, N_\theta, \beta=0} (v_\beta \cdot S_3)} \quad (16)$$

$$N_\gamma = \frac{\sum_{N_\beta, N_\gamma, N_\theta} (v_\gamma \cdot \delta V)}{D \cdot \sum_{N_\beta, N_\theta, \beta=0} (v_\beta \cdot S_3)} \quad (17)$$

$$N_c = \frac{\sum_{N_\beta, N_\gamma, N_\theta} (2 \cdot \max(|\varepsilon_i|) \cdot \delta V)}{\sum_{N_\beta, N_\theta, \beta=0} (v_\beta \cdot S_3)} \quad (18)$$

$$N_{kh} = \frac{\sum_{N_\beta, N_\gamma, N_\theta} \left\{ \left[1 + \frac{C+D+y_i}{C+D} \cdot (f-1) \right] \cdot k_h \cdot \sin 2\pi \left(\frac{t}{T} - \frac{C+D+y_i}{TV_s} \right) \cdot v_z \cdot \delta V \right\}}{D \cdot \sum_{N_\beta, N_\theta, \beta=0} (v_\beta \cdot S_3)} \quad (19)$$

$$N_{kv} = \frac{\sum_{N_\beta, N_\gamma, N_\theta} \left\{ \left[1 + \frac{C+D+y_i}{C+D} \cdot (f-1) \right] \cdot k_v \cdot \sin 2\pi \left(\frac{t}{T} - \frac{C+D+y_i}{TV_p} + \frac{t_0}{T} \right) \cdot v_y \cdot \delta V \right\}}{D \cdot \sum_{N_\beta, N_\theta, \beta=0} (v_\beta \cdot S_3)} \quad (20)$$

The collapse support pressures calculated through Eq. (15) are variational and associated with time t . By means of an unconstrained optimization tool called "fminsearch" in MATLAB, the maximum of the collapse support pressures can be achieved and is considered as the critical collapse support pressure.

Base on upper-bound theorem in the framework of

kinematic analysis, note that the collapse support pressure calculated by Eq. (15) is actually a rigorous lower bound of the real critical collapse pressure because the direction of the support pressure on tunnel face is opposite to the direction of the velocity of soils.

3.2 Pseudo-static stability analysis

For comparison purpose, the pseudo-static approach is also adopted in the present work. The conventional pseudo-static approach doesn't take into account time effect and spatial effect such as the amplification phenomenon of the seismic wave. Under some circumstances, the conventional pseudo-static approach even ignores the influence of vertical seismic waves because Chen and Liu (1990) reported that the effects generated by the vertical component of seismic forces are generally negligible. However, many investigators believed the vertical effects should be considered when the horizontal seismic acceleration is relatively large.

Due to non-consideration of time effect and spatial effect, the horizontal and vertical seismic effects can be simply expressed by seismic coefficients k_h and k_v , both of which are constants. Therefore, the horizontal and vertical seismic accelerations are $k_h g$ and $k_v g$ and remain unchanging throughout the soil. Similar to the pseudo-dynamic stability analysis, by combining the pseudo-static approach with the advanced 3D failure mechanism in **Section 2**, the collapse support pressure is obtained via Eq. (15) except that the N_{kh} and N_{kv} are given by

$$N_{kh} = \frac{\sum_{N_\beta, N_r, N_\theta} (k_h \cdot v_z \cdot \delta V)}{D \cdot \sum_{N_r, N_\theta, \beta=0} (v_\beta \cdot S_3)} \quad (21)$$

$$N_{kv} = \frac{\sum_{N_\beta, N_r, N_\theta} (k_v \cdot v_y \cdot \delta V)}{D \cdot \sum_{N_r, N_\theta, \beta=0} (v_\beta \cdot S_3)} \quad (22)$$

The other dimensionless coefficients N_s , N_γ and N_c have the same expressions as Eq. (16), Eq. (17) and Eq. (18), respectively. In this way, in the framework of kinematic analysis associated with the pseudo-static approach, a rigorous lower bound of critical collapse support pressure is obtained, too.

4. Validation

The literature related to seismic stability analysis of a tunnel face in purely cohesive soils is scarce and no previous research results are available for comparison. To validate the proposed mechanism, it is necessary to conduct a numerical simulation for comparison. However, the pseudo-dynamic approach is time dependent and involves an optimized searching for the most unstable state. For numerical simulations, the characteristic of time-consuming computation makes it impossible to implement such a searching process. For this reason, only one moment that $t=0$ is considered in present numerical models. The profile

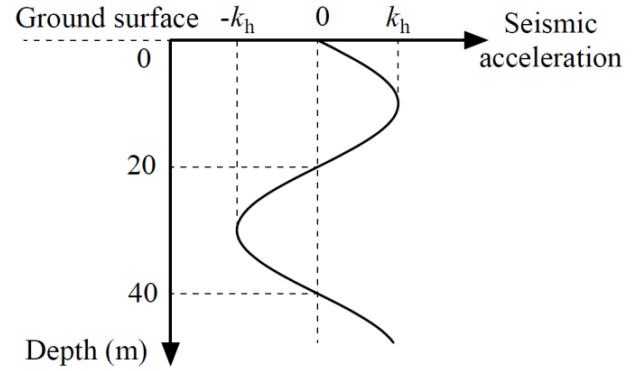


Fig. 3 Profile of the acceleration with depth

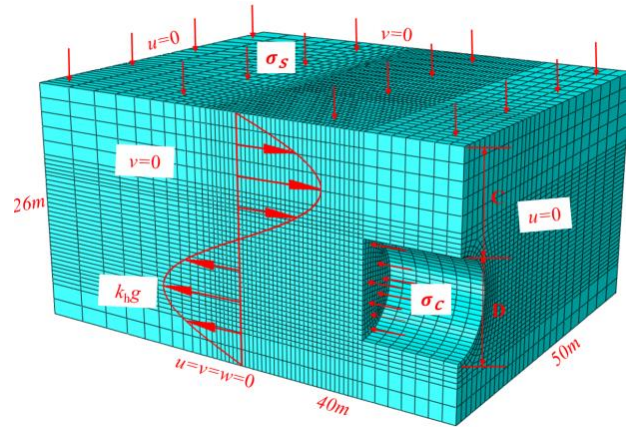


Fig. 4 Numerical model for the analysis of face collapse

of the acceleration with the depth is shown in Fig. 3.

A numerical model of a circular tunnel with diameter $D=10$ m and cover depth $C=10$ m is constructed in ABAQUS software, as shown in Fig. 4. Only half of the relevant region is modelled due to the symmetry. Mollon *et al.* (2013) had also conducted a numerical model for a tunnel whose size is $C=10$ m and $D=10$ m. The size of that model was 50 m \times 40 m \times 26 m in transversal, longitudinal and vertical directions respectively, and had been proved sufficient enough to avoid the influence of boundary conditions. Therefore, same size is adopted for the numerical model here. The soil is regarded as elastic perfectly plastic material and subjected to Tresca failure criterion. The properties of soil are set as follows: Young's Modulus $E=240$ MPa, Poisson's ratio $\nu=0.49$, undrained cohesion $c_u=20$ kPa and 30 kPa. A very high value of Young's Modulus is selected to acquire a higher computational efficiency without influencing the results required (Ukritchon *et al.* 2017).

In this model, the horizontal seismic force is inserted in a sinusoidal way as Eq. (9) but the value of time parameter t is fixed as 0 . Moreover, the vertical seismic effect is not considered. The other seismic parameters are set as follows: $T=0.2$ s, $V_s=200$ m/s, $k_h=0$ to 0.2 . The upper end of k_h is limited to 0.2 because a higher value of k_h would lead to severe distortion of soil elements and the solver of ABAQUS aborts.

To simulate the collapse process of tunnel face during

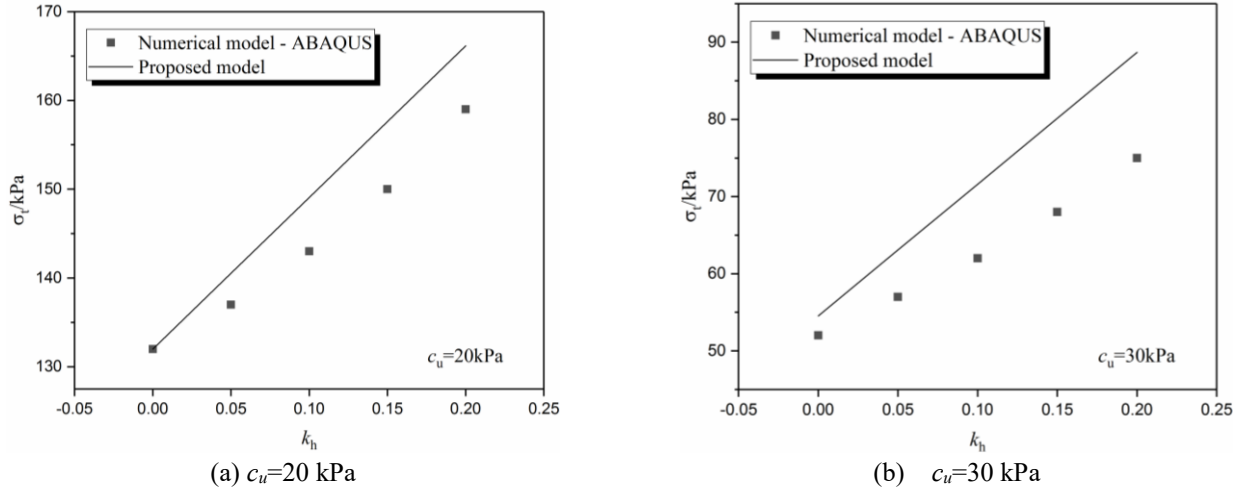


Fig. 5 Comparison of critical collapse support pressures provided by proposed mechanism and numerical simulations

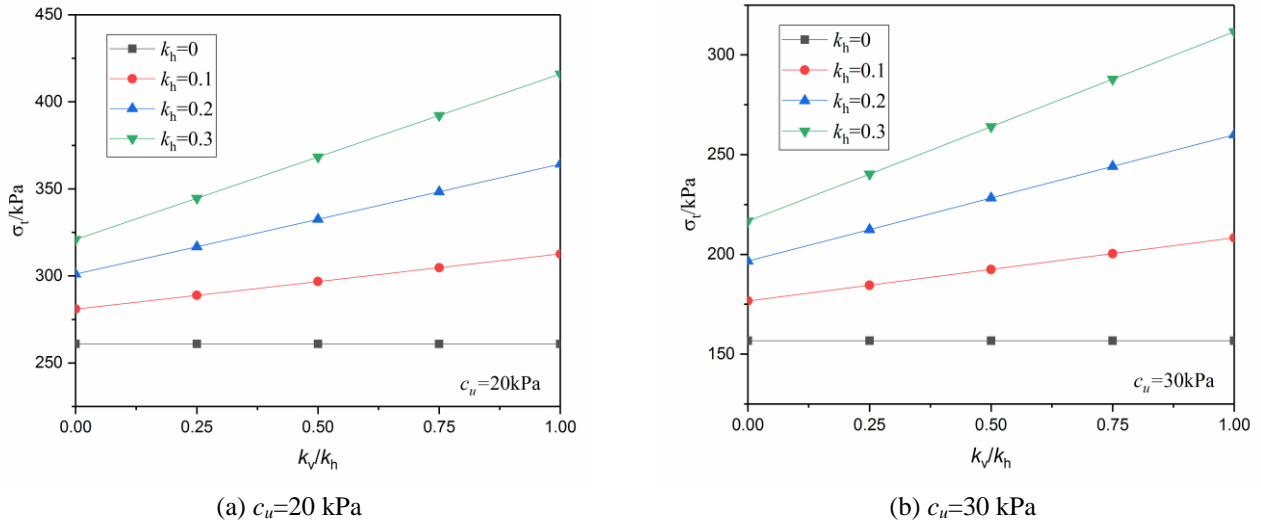


Fig. 6 Effect of vertical seismic coefficient on critical collapse support pressures

the excavation, the soil mass ahead of tunnel face is simply removed in an instant and the lining of tunnel is fully fixed in all directions. These assumptions are reasonable in that the purpose of present work is to investigate the tunnel face. When this numerical model is used to determine the critical collapse support pressure, the process is just the same as Huang *et al.* (2019): the pressure applied on tunnel face is set at a relatively high value at the beginning, ensuring that the collapse doesn't occur; then the pressure begins to decrease in a rapid way until the soils of tunnel face appear big displacement; next, the pressure decreases in a slight way in order to guarantee the precision of critical collapse pressure obtained; finally, when the displacement of a characteristic node in tunnel face increases sharply and the ABAQUS solver fails to converge, the pressure applied is regarded as the critical collapse support pressure. In this way, the critical pressures by numerical models are obtained and plotted in Fig. 5 together with results by proposed model for comparison.

In Fig. 5, it can be seen that the results obtained by proposed mechanism and numerical simulations have a similar trend with the variation of k_h . The critical collapse

support pressure provided by proposed mechanism increases linearly with increasing k_h and the critical collapse support pressure provided by numerical simulations increases approximately in a linear mode too. However, the slopes of them are not the same value, resulting in that the biggest differences of results between these two methods reach 4.30% and 14.30% in condition of $c_u = 20$ kPa and $c_u = 30$ kPa respectively when the value of k_h is 0.2. This indicates that the proposed model is more effective in soils with a lower cohesion. In general, according to Fig. 5, the differences of results between proposed mechanism and numerical simulation are limited at an acceptable level and the proposed mechanism could provide an effective prediction of critical collapse support pressure, especially in condition of lower c_u and k_h .

5. Numerical results

By the kinematic analysis with a pseudo-dynamic approach, the lower bound of critical collapse support pressure is obtained. The numerical results focus on the

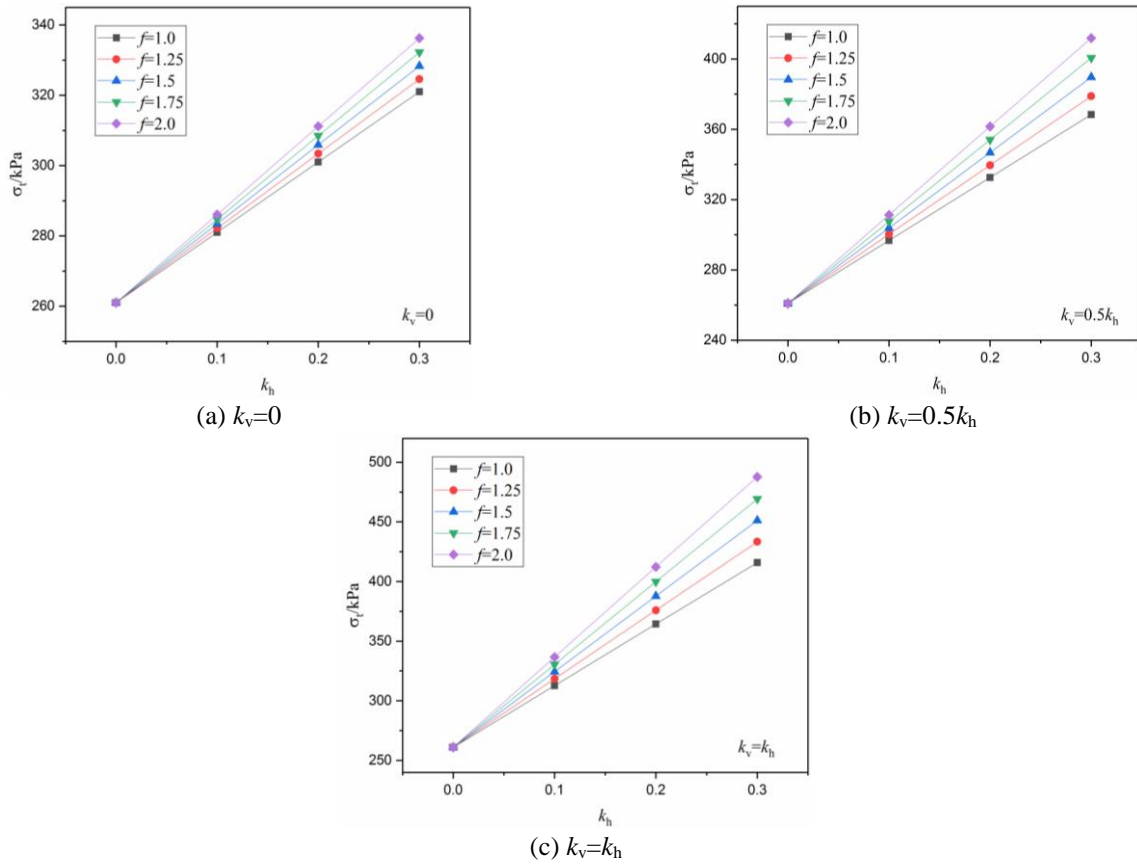


Fig. 7 Effect of soil amplification factor on critical collapse support pressures

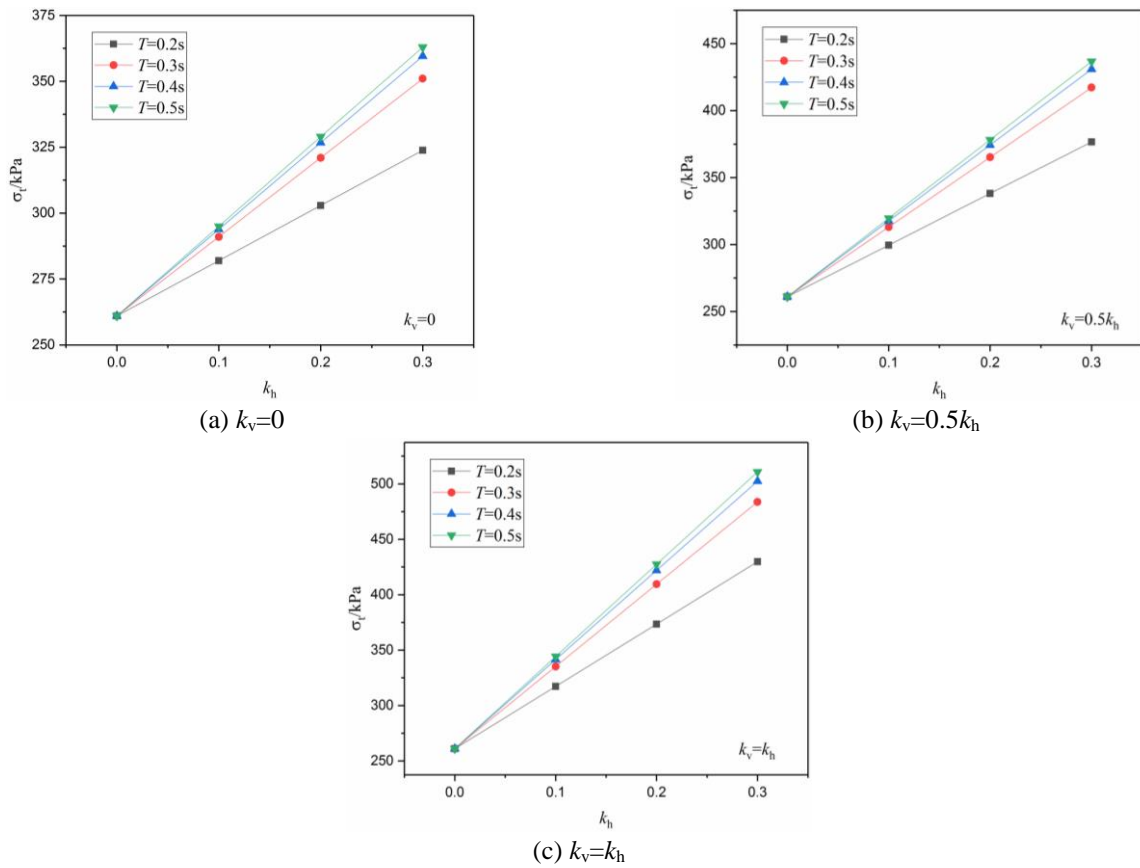


Fig. 8 Effect of seismic wave period on critical collapse support pressures

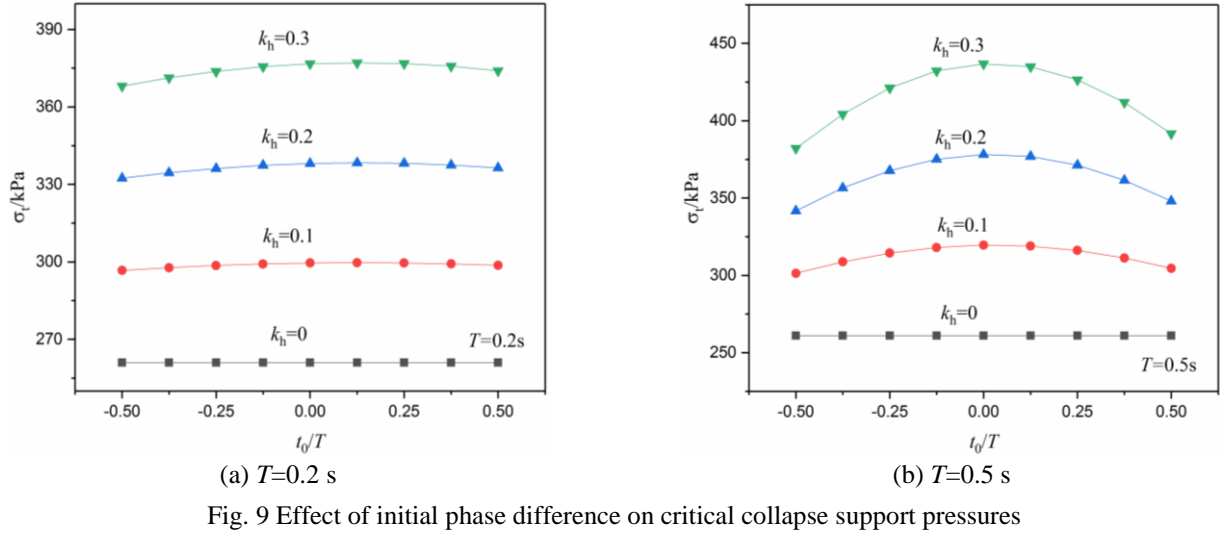


Fig. 9 Effect of initial phase difference on critical collapse support pressures

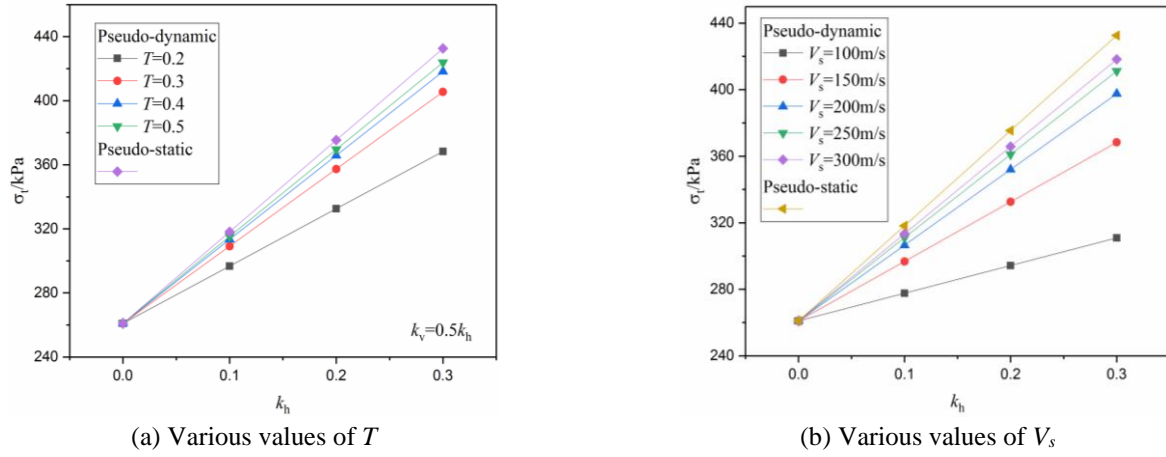


Fig. 10 Comparison of pseudo-dynamic/static approaches

effects of the vertical seismic coefficient k_v , soil amplification factor f , seismic wave period T and initial phase difference t_0 on the collapse support pressure. In addition, the difference between pseudo-dynamic approach and pseudo-static approach is carefully investigated and the applicable conditions of these two methods would be discussed.

5.1 Parametric analysis

5.1.1 Effect of vertical seismic coefficient k_v

To analyze the vertical seismic effect, Fig. 6 shows the values of critical collapse support pressure for various ratios of the vertical seismic coefficient to the horizontal seismic coefficient with $C=20$ m, $D=10$ m, $c_u=20$ KPa or 30 kPa, $V_s=150$ m/s, $V_p=280.5$ m/s, $T=0.2$ s, $t_0=0$ s and $f=1.0$. As expected, the effect of vertical seismic coefficient do could be neglected when the horizontal seismic coefficient is small. For example, if the value of k_h is 0.1, Fig. 6 illustrates that the differences of the critical collapse support pressures between taking account of $k_v/k_h=0.5$ and taking no account of the k_v would be 5.62% in the condition of $c_u=20$ KPa and 8.93% in the condition of $c_u=30$ KPa. Hence, without consideration of k_v wouldn't cause a big error under this circumstance. However, with the increase of k_h , the

effect of k_v would be significant. From Fig.6, in the case of $k_h=0.3$, the critical collapse support pressure considering $k_v/k_h=0.5$ would be 14.75% and 21.85% more than not considering k_v in the condition of $c_u=20$ KPa and $c_u=30$ KPa respectively. If the vertical seismic motion is drastic and the value of k_v rises to the same as k_h , the differences would even reach up to 29.57% and 43.81%. Obviously, the vertical seismic effect shouldn't be ignored in these circumstances and without consideration of k_v may lead to the occurrence of a tunnel face collapse. In general, a conclusion can be drawn that it is necessary to take into account the effect of vertical seismic motion for much safer construction.

5.1.2 Effect of soil amplification factor f

To analyze the effect of soil amplification factor, Fig. 7 shows the variation of critical collapse support pressure with different values of soil amplification factor (f) for $C=20$ m, $D=10$ m, $c_u=20$ kPa, $V_s=150$ m/s, $V_p=280.5$ m/s, $T=0.2$ s, $t_0=0$ s and $k_v/k_h=0, 0.5$ and 1.0. From the results presented, it is obvious that the effect of soil amplification factor has a close connection with the magnitude of k_h and k_v . In the case of $k_h=0.3$ and $k_v=0$, the increment of critical collapse support pressure is 4.75% when f changes from 1.0 to 2.0, which is a marginal number. In contrast, the increment of critical collapse support pressure reaches

17.27% in the case of $k_h=0.3$ and $k_v=k_h$ when f changes from 1.0 to 2.0. Therefore, the effect of soil amplification factor deserves particular consideration in areas where earthquakes are intense.

5.1.3 Effect of seismic wave period T

To analyze the effect of seismic wave period, Fig. 8 presents the variation of critical collapse support pressure with different values of seismic wave period (T) for $C=20$ m, $D=10$ m, $c_u=20$ kPa, $V_s=150$ m/s, $V_p=280.5$ m/s, $f=1.2$, $t_0=0$ s and $k_v/k_h=0, 0.5$ and 1.0 . As can be seen from these figures, no matter what values of k_h and k_v are, the critical collapse support pressure seems to gradually approach a certain value with the growth of T . Taking the case of $k_h=3.0$ and $k_v=0$ as an example, when T increases from 0.2 s to 0.3 s, the critical collapse support pressure increases by 10.78%; when T increases from 0.4 s to 0.5 s, the critical collapse support pressure increases only by 1.36%. Along with this trend, the critical collapse support pressure would definitely converge to a certain value when T continues to grow. Therefore, the critical collapse support pressure is more susceptible to T when the value of T is relatively small and gradually approaches a certain value when the value of T is increasingly large.

5.1.4 Effect of initial phase difference t_0

To analyze the effect of initial phase difference, Fig. 9 gives the critical collapse support pressure for different t_0 with $C=20$ m, $D=10$ m, $c_u=20$ kPa, $V_s=150$ m/s, $V_p=280.5$ m/s, $f=1.2$, $T=0.2$ s and 0.5 s, $k_h=0, 0.1, 0.2$ and 0.3 and $k_v=0.5k_h$. The Figs. 9 (a) and (b) illustrate that the effect of t_0 has a periodic pattern and susceptible to the values of k_h and T . With larger values of k_h and T , the difference of critical collapse support pressures among situations of various t_0/T would significantly increase. In the case of $k_h=0.3$ and $T=0.5$ s, when t_0/T increases from -0.5 to 0, the value of σ_t increases by 14.32%. This demonstrates that the decision of an exact value of t_0 is necessary for more accurate critical collapse support pressure determination.

5.2 Comparison with pseudo-static approach

Before the present work, many investigators have already made comparisons between pseudo-dynamic approach and pseudo-static approach and many effective results have been obtained. However, most of them just showed the differences between results obtained through these two approaches and the essential mechanism which gives rise to these differences hasn't been investigated yet. To reveal this internal mechanism, an in-depth study on it is necessary to be conducted.

5.2.1 Results comparison

Firstly, without regard to the soil amplification factor, Figs. 10(a) and (b) present the variation of critical collapse support pressure with different values of T and V_s corresponding to pseudo-dynamic approach respectively. For comparison, the results obtained through pseudo-static approach are also plotted on these two figures. The values of related parameters in Fig 10(a) are $C=20$ m, $D=10$ m,

$c_u=20$ kPa, $V_s=100$ m/s, $V_p=1.87V_s$, $k_h=0, 0.1, 0.2$ and 0.3 , $k_v=0.5k_h$, and $T=0.2$ s to 0.5 s. The parameters in Fig. 10(b) are the same as Fig. 10(a) except that $V_s=100$ m/s to 300 m/s and $T=0.2$ s. From Fig. 10(a), with an increase of T in pseudo-dynamic approach, the support pressure needed to maintain face stability is increasing but never exceeds the results obtained by pseudo-static approach. The difference between results obtained by pseudo-dynamic and pseudo-static approaches decreases gradually as T increases. Based on this trend, a reasonable conjecture can be made that the results obtained by pseudo-dynamic approach would converge to the corresponding results obtained by pseudo-static approach if T continues to increase and reaches to infinity. A similar trend can be found in Fig. 10(b) too. From Fig. 10(b), as V_s increases, results obtained by pseudo-dynamic approach gradually converge to those obtained by pseudo-static approach. Note that both T and V_s are associated with the wavelength of the shear wave (λ_s) because of $\lambda_s=TV_s$. Therefore, there is an intimate connection between the seismic wavelength and the results of pseudo-dynamic approach.

5.2.2 Revelation of mechanism

To reveal the mechanism of pseudo-dynamic approach in kinematic analysis, a simplest case is chosen for analysis as shown in Fig. 11. In the framework of kinematic approach, the seismic effect is accounted for by means of seismic work rate which is generated by the seismic acceleration. For the pseudo-dynamic approach, the seismic acceleration is a sinusoidal function correlated with time; while for the pseudo-static approach, the seismic acceleration is a constant. In Fig. 11(a), there is a soil failure body whose horizontal and vertical dimensions are l and 2π respectively. Considering the simplest velocity field and all particles of this soil failure body are assumed to have the same horizontal velocity v . Figs. 11(b) to (f) show the distribution of seismic acceleration (a_s) in pseudo-static approach and pseudo-dynamic approach.

As for pseudo-static approach, with non-consideration of time and space effect, the seismic acceleration at any time and any position of the soil failure body is the same constant ag as shown in Fig. 11(b). As for pseudo-dynamic approach, the seismic acceleration propagates from the bottom of the soil failure body to the top with the form of a sinusoidal function which is time-related. Figs. 11(c) to 11(f) plot the distribution of seismic acceleration at a certain moment when the seismic work rate is maximal. Different wavelengths of the seismic wave such as $2\pi, 4\pi, 8\pi$ and 16π are chosen for comparison. The detailed calculating formulas and results of seismic work rate are presented in Table 1.

From Table 1, it can be inferred that the ratio between seismic wavelength and height of failure body has a significant effect on results obtained from pseudo-dynamic approach. In this case, with a certain $h=2\pi$ and λ ranging from 2π to 16π , the seismic work rate by pseudo-dynamic approach increases substantially and gradually gets close to that obtained by pseudo-static approach. When the value of λ is 16π , the seismic work rate obtained by pseudo-dynamic approach even reaches up to 97.45% of that obtained by pseudo-static approach. The mechanism resulting in this

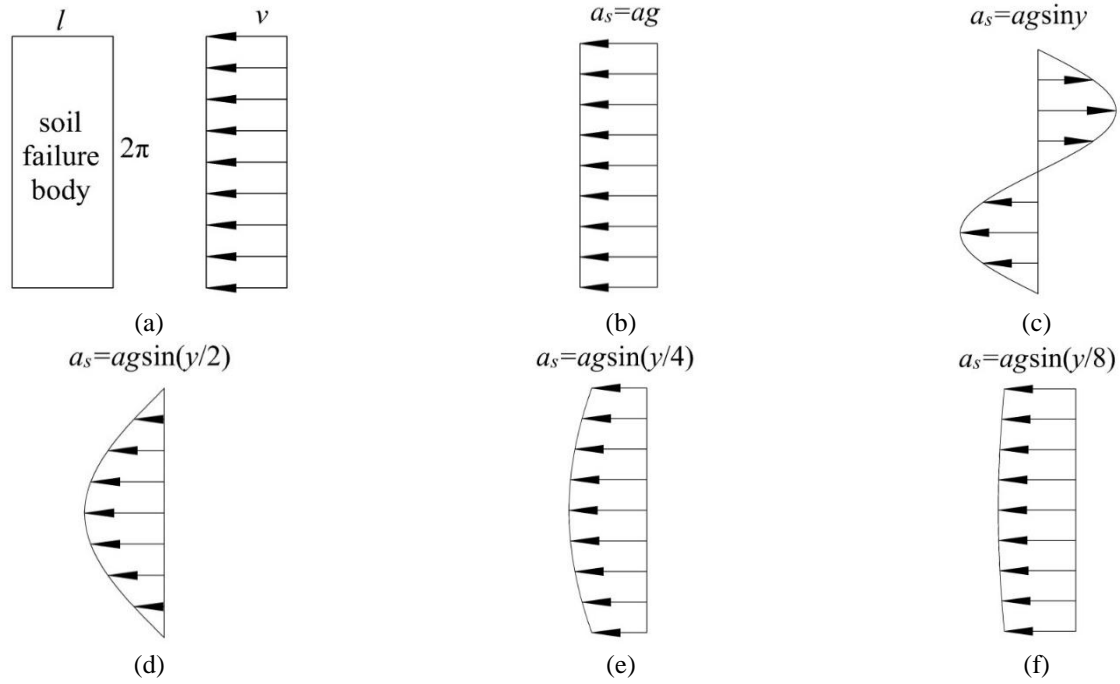


Fig. 11 Comparison of pseudo-dynamic/static approaches for a simplest case: (a) velocity field of a soil failure body, (b) seismic acceleration of pseudo-static approach and (c)-(f) seismic acceleration of pseudo-dynamic approach with various seismic wavelengths

Table 1 Comparison of seismic work rate by pseudo-dynamic/static approaches for a simplest case

Item	Pseudo-static	Pseudo-dynamic				
		$\lambda=2\pi$	$\lambda=4\pi$	$\lambda=8\pi$	$\lambda=16\pi$	
Wavelength/Height ($\frac{\lambda}{h}$)	—	1	2	3	4	
Formula	$2\pi agvl$	$\int_0^{2\pi} ag \sin y dy$	$\int_0^{2\pi} ag \sin \frac{y}{2} dy$	$\int_{\pi}^{3\pi} ag \sin \frac{y}{4} dy$	$\int_{3\pi}^{5\pi} ag \sin \frac{y}{8} dy$	
Seismic work rate	Result	$2\pi agvl$	0	$4agvl$	$4\sqrt{2}agvl$	$8\sqrt{2-\sqrt{2}}agvl$
Pseudo-dynamic / Pseudo-static $\times 100\%$	—	0	63.66%	90.03%	97.45%	

kind of phenomenon can be well illustrated in Fig. 11. For a certain velocity field, the seismic acceleration at any point of the failure body reaches the maximal value ag in pseudo-static approach as shown in Fig. 11(b). However, in the pseudo-dynamic approach shown in Figs. 11(c) to (f), the seismic accelerations in different elevations range from $-ag$ to ag no matter which moment is considered. Thus, without considering the soil amplification factor, the seismic work rate obtained by pseudo-static approach would definitely be bigger than pseudo-dynamic approach, which implies that the pseudo-static approach is a relatively conservative method compared to pseudo-dynamic approach.

Moreover, if the seismic wavelength is much bigger than the height of a considered structure, the difference between pseudo-static approach and pseudo-dynamic approach at the most unstable situation would be very tiny. In Fig. 11(f), the seismic wavelength is four times longer than the height of the soil failure body and this results in that the seismic acceleration among this height can be very close to the maximal value ag at a certain moment. Before the present work, many investigators have already taken the

pseudo-dynamic and pseudo-static approach for comparison in the framework of kinematic approach but the difference of results obtained was not significant. This phenomenon perhaps could be attributed to that the size of the considered structure is too small or the value of seismic wavelength is too large. For example, the height of slope studied by Qin and Chian (2017) is only 8 m but the value of shear wavelength and primary wavelength are 30 m and 56.1 m respectively. The seismic wavelengths in Qin and Chian (2017) are several times more than the height of failure soil structure so that the maximum difference obtained by pseudo-dynamic approach and pseudo-static approach is only 4.17%.

Of course, the velocity field in Fig. 11 is pretty simple and the actual velocity field would be much complex: the magnitude, direction and concentration of velocity could be various; the seismic wave could include both shear wave and primary wave and between them there could be an initial phase difference t_0 . However, no matter how complex the actual velocity field is, such a velocity field can be regarded as consisting of plenty of simple velocity fields

like Fig. 11(a). Thus, the actual velocity fields would have a similar law. Namely, in the framework of kinematic approach, a conclusion could be drawn that the pseudo-static approach is more conservative than the pseudo-dynamic approach and the results obtained by pseudo-dynamic approach are increasingly close to those by pseudo-static approach with increasing ratio of the seismic wavelength to the height of a structure. Similar results can also be found in previous literature which implemented these two seismic approaches in other geotechnical engineering such as retaining walls (Chehade *et al.* 2019, Chehade *et al.* 2020).

6. Limitation

There is no available literature about the seismic stability analysis of tunnel face in purely cohesive soils and the present work can be seen as a pioneering study in this field, so comparisons with results by other investigators cannot be implemented. Besides, the effect of an earthquake on structures cannot be fully accounted for only by seismic accelerations. The properties of soils would also be degraded by seismic waves and the velocity fields would subsequently change. In the present work, both the soil property and the velocity field are assumed as unchanging. For this reason, the objective of the present work is not to provide practical charts for actual design or construction. Emphasis is laid on an in-depth study about the application of pseudo-dynamic approach in limit analysis. Further investigations should be made before the results could be directly used to guide practical engineering.

7. Conclusions

Considering both the time and space effect of seismic motion, the seismic stability of tunnel face in purely cohesive soils is studied by the combination of an advanced 3D failure mechanism in the framework of kinematic approach and the pseudo-dynamic approach. Based on this study, two major conclusions could be drawn as follows.

- The pseudo-dynamic approach takes into account the seismic effect by means of the earthquake-induced acceleration with a sinusoidal function. Results obtained through this approach demonstrate that the vertical seismic coefficient, soil amplification factor, seismic wave period and initial phase difference of pseudo-dynamic approach have significant effects on the determination of the critical collapse support pressure of tunnel face, especially when the value of horizontal seismic coefficient is relatively large.
- By comparing the implementation of pseudo-dynamic approach and pseudo-static approach in limit analysis, the pseudo-dynamic approach can better represent the actual earthquake conditions for its excellent description of characteristics of seismic waves. On the contrary, the pseudo-static approach simply assumes that all parts of the structure suffer the maximal value of seismic waves, and therefore it is a conservative method. Without considering

the soil amplification factor, the critical collapse support pressure calculated by pseudo-dynamic approach wouldn't exceed that by pseudo-static approach. However, if the seismic wavelength is much bigger than the height of structure, the difference of results obtained by both approaches would be really tiny. In this case, the pseudo-static approach is still a simple and efficient way to evaluate seismic effect.

Acknowledgments

This research was supported by the Jiangxi Provincial Department of Communications Key Technology Foundation (No. 2020Z0001 and 2016C0007).

References

- Aksoy, C.O., Aksoy, G.U., Guney, A., Ozacar, V. and Yaman, H.E. (2020), "Influence of time-dependency on elastic rock properties under constant load and its effect on tunnel stability", *Geomech. Eng.*, **20**(1), 1-7. <http://doi.org/10.12989/gae.2020.20.1.001>.
- Basha, B.M. and Babu, G.S. (2009), "Computation of sliding displacements of bridge abutments by pseudo-dynamic method", *Soil Dyn. Earthq. Eng.*, **29**(1), 103-120. <https://doi.org/10.1016/j.soildyn.2008.01.006>.
- Chehade, H.A., Dias, D., Sadek, M., Jenck, O. and Chehade, F.H. (2019), "Seismic analysis of geosynthetic-reinforced retaining wall in cohesive soils", *Geotext. Geomembr.*, **47**(3), 315-326. <https://doi.org/10.1016/j.geotextmem.2019.02.003>.
- Chehade, H.A., Dias, D., Sadek, M., Jenck, O. and Chehade, F.H. (2020), "Upper bound seismic limit analysis of geosynthetic-reinforced unsaturated soil walls", *Geotext. Geomembr.*, **48**(4), 419-430. <https://doi.org/10.1016/j.geotextmem.2020.02.001>.
- Chen, G.H., Zou, J.F. and Chen, J.Q. (2019), "Shallow tunnel face stability considering pore water pressure in non-homogeneous and anisotropic soils", *Comput. Geotech.*, **116**, 103205. <https://doi.org/10.1016/j.compgeo.2019.103205>.
- Chen, G.H., Zou, J.F., Pan, Q.J., Qian, Z.H. and Shi, H.Y. (2020), "Earthquake-induced slope displacements in heterogeneous soils with tensile strength cut-off", *Comput. Geotech.*, **124**, 103637. <https://doi.org/10.1016/j.compgeo.2020.103637>.
- Chen, W.F. (1975), *Limit Analysis and Soil Plasticity*, Elsevier, Amsterdam, The Netherlands.
- Chen, W.F. and Liu, X.L. (1990), *Limit Analysis in Soil Mechanics*, Elsevier, Amsterdam, The Netherlands.
- Das, B.M. (1993), *Principles of Soil Dynamics*, PWS-KENT Publishing Company, Boston, Massachusetts, U.S.A.
- Ganesh, R., Khuntia, S. and Sahoo, J.P. (2018), "Seismic uplift capacity of shallow strip anchors: A new pseudo-dynamic upper bound limit analysis", *Soil Dyn. Earthq. Eng.*, **109**, 69-75. <https://doi.org/10.1016/j.soildyn.2018.03.004>.
- Giri, D. (2011), "Pseudo-dynamic approach of seismic earth pressure behind cantilever retaining wall with inclined backfill surface", *Geomech. Eng.*, **3**(4), 255-266. <https://doi.org/10.12989/gae.2011.3.4.255>.
- Huang, Q., Zou, J.F. and Qian, Z.H. (2019), "Face stability analysis for a longitudinally inclined tunnel in anisotropic cohesive soils", *J. Central South Univ.*, **26**(7), 1780-1793. <https://doi.org/10.1007/s11771-019-4133-4>.
- Klar, A. and Klein, B. (2014), "Energy-based volume loss prediction for tunnel face advancement in clays", *Géotechnique*, **64**(10), 776-786. <https://doi.org/10.1680/geot.14.P.024>.

- Klar, A., Osman, A.S. and Bolton, M. (2007), "2D and 3D upper bound solutions for tunnel excavation using 'elastic' flow fields", *Int. J. Numer. Anal. Meth. Geomech.*, **31**(12), 1367-1374. <https://doi.org/10.1002/nag.597>.
- Li, C. and Zou, J.F. (2019), "Anisotropic elasto-plastic solutions for cavity expansion problem in saturated soil mass", *Soils Found.*, **59**(5), 1313-1323. <https://doi.org/10.1016/j.sandf.2019.05.012>.
- Li, T.Z. and Yang, X.L. (2019), "Face stability analysis of rock tunnels under water table using Hoek-Brown failure criterion", *Geomech. Eng.*, **18**(3), 235-245. <https://doi.org/10.12989/gae.2019.18.3.235>.
- Liu, X.R., Li, D.L., Wang, J.B. and Wang, Z. (2015), "Surrounding rock pressure of shallow-buried bilateral bias tunnels under earthquake", *Geomech. Eng.*, **9**(4), 427-445. <https://doi.org/10.12989/gae.2015.9.4.427>.
- Mollon, G., Dias, D. and Soubra, A.H. (2013), "Continuous velocity fields for collapse and blowout of a pressurized tunnel face in purely cohesive soil", *Int. J. Numer. Anal. Meth. Geomech.*, **37**(13), 2061-2083. <https://doi.org/10.1002/nag.2121>.
- Osman, A.S., Mair, R.J. and Bolton, M.D. (2006), "On the kinematics of 2D tunnel collapse in undrained clay", *Géotechnique*, **56**(9), 585-595. <https://doi.org/10.1680/geot.2006.56.9.585>.
- Pan, Q. and Dias, D. (2018), "Three-dimensional static and seismic stability analysis of a tunnel face driven in weak rock masses", *Int. J. Geomech.*, **18**(6), 04018055. [https://doi.org/10.1061/\(ASCE\)GM.1943-5622.0001174](https://doi.org/10.1061/(ASCE)GM.1943-5622.0001174).
- Pan, Q.J. and Dias, D. (2015), "Face stability analysis for a shield-driven tunnel in anisotropic and nonhomogeneous soils by the kinematical approach", *Int. J. Mech.*, **16**(3), 04015076. [https://doi.org/10.1061/\(ASCE\)GM.1943-5622.0000569](https://doi.org/10.1061/(ASCE)GM.1943-5622.0000569).
- Perazzelli, P. and Anagnostou, G. (2017), "Analysis method and design charts for bolt reinforcement of the tunnel face in purely cohesive soils", *J. Geotech. Geoenviron. Eng.*, **143**(9), 04017046. [https://doi.org/10.1061/\(ASCE\)GT.1943-5606.0001702](https://doi.org/10.1061/(ASCE)GT.1943-5606.0001702).
- Prakash, S. (1981), *Soil Dynamics*, McGraw-Hill Companies, New York, U.S.A.
- Qian, Z.H., Zou, J.F., Pan, Q.J. and Dias, D. (2019), "Safety factor calculations of a tunnel face reinforced with umbrella pipes: A comparison analysis", *Eng. Struct.*, **199**, 109639. <https://doi.org/10.1016/j.engstruct.2019.109639>.
- Qian, Z.H., Zou, J.F., Tian, J. and Pan, Q.J. (2020), "Estimations of active and passive earth thrusts of non-homogeneous frictional soils using a discretisation technique", *Comput. Geotech.*, **119**, 103366. <https://doi.org/10.1016/j.compgeo.2019.103366>.
- Qin, C.B. and Chian, S.C. (2017), "Kinematic analysis of seismic slope stability with a discretisation technique and pseudo-dynamic approach: a new perspective", *Géotechnique*, **68**(6), 492-503. <https://doi.org/10.1680/jgeot.16.P.200>.
- Saada, Z., Maghous, S. and Garnier, D. (2013), "Pseudo-static analysis of tunnel face stability using the generalized Hoek-Brown strength criterion", *Int. J. Numer. Anal. Meth. Geomech.*, **37**(18), 3194-3212. <https://doi.org/10.1002/nag.2185>.
- Schofield, A.N. (1980), "Cambridge geotechnical centrifuge operations", *Geotechnique*, **30**(3), 227-268. <https://doi.org/10.1680/geot.1980.30.3.227>.
- Shukla, R.P. and Jakka, R.S. (2018), "Critical setback distance for a footing resting on slopes under seismic loading", *Geomech. Eng.*, **15**(6), 1193-1205. <https://doi.org/10.12989/gae.2018.15.6.1193>.
- Steedman, R.S. and Zeng, X. (1990), "The influence of phase on the calculation of pseudo-static earth pressure on a retaining wall", *Géotechnique*, **40**(1), 103-112. <https://doi.org/10.1680/geot.1990.40.1.103>.
- Sun, Q.Q. and Dias, D. (2019), "Assessment of stress relief during excavation on the seismic tunnel response by the pseudo-static method", *Soil Dyn. Earthq. Eng.*, **117**, 384-397. <https://doi.org/10.1016/j.soildyn.2018.09.019>.
- Ukritchon, B., Yingchaloenkitkhajorn, K. and Keawsawasvong, S. (2017), "Three-dimensional undrained tunnel face stability in clay with a linearly increasing shear strength with depth", *Comput. Geotech.*, **88**, 146-151. <https://doi.org/10.1016/j.compgeo.2017.03.013>.
- Wang, L., Zou, J.F., Yang, T. and Wang, F. (2019), "Elastic solutions for shallow tunnels excavated under non-axisymmetric displacement boundary conditions on a vertical surface", *Geomech. Eng.*, **19**(3), 201-215. <https://doi.org/10.12989/gae.2019.19.3.201>.
- Xue, Y., Li, X., Qiu, D., Ma, X., Kong, F., Qu, C. and Zhao, Y. (2019), "Stability evaluation for the excavation face of shield tunnel across the Yangtze River by multi-factor analysis", *Geomech. Eng.*, **19**(3), 283-293. <https://doi.org/10.12989/gae.2019.19.3.283>.
- Zhang, B., Wang, X., Zhang, J.S. and Meng, F. (2017), "Three-dimensional limit analysis of seismic stability of tunnel faces with quasi-static method", *Geomech. Eng.*, **13**(2), 301-318. <https://doi.org/10.12989/gae.2017.13.2.301>.
- Zhang, F., Gao, Y.F., Wu, Y.X. and Zhang, N. (2017), "Upper-bound solutions for face stability of circular tunnels in undrained clays", *Géotechnique*, **68**(1), 76-85. <https://doi.org/10.1680/jgeot.16.T.028>.
- Zou, J.F. and Qian, Z.H. (2018), "Face-stability analysis of tunnels excavated below groundwater considering coupled flow deformation", *Int. J. Geomech.*, **18**(8), 04018089. [https://doi.org/10.1061/\(ASCE\)GM.1943-5622.0001199](https://doi.org/10.1061/(ASCE)GM.1943-5622.0001199).
- Zou, J.F., and Zuo, S.Q. (2017), "Similarity solution for the synchronous grouting of shield tunnel under the vertical non-axisymmetric displacement boundary condition", *Adv. Appl. Math. Mech.*, **9**(1), 205-232. <https://doi.org/10.4208/aamm.2016.m1479>.
- Zou, J.F., Qian, Z.H., Xiang, X.H. and Chen, G.H. (2019), "Face stability of a tunnel excavated in saturated nonhomogeneous soils", *Tunn. Undergr. Sp. Tech.*, **83**, 1-17. <https://doi.org/10.1016/j.tust.2018.09.007>.

CC